Above-Threshold Effects in the Photodissociation and Photoionization of Iodobenzene[†]

Sujatha Unny, Yan Du, Langchi Zhu, Kaspars Truhins, and Robert J. Gordon*

Department of Chemistry (m/c 111), University of Illinois at Chicago, 845 West Taylor Street, Chicago, Illinois 60607-7061

Akihiro Sugita and Masahiro Kawasaki

Department of Molecular Engineering, Kyoto University, Kyoto 606-8501, Japan

Y. Matsumi

Solar Terrestrial Environment Laboratory, Nagoya University, Toyokawa 442-8505, Japan

Ralph Delmdahl and David H. Parker

Department of Molecular and Laser Physics, University of Nijmegen, Toernooiveld 1, 6523 ED Nijmegen, The Netherlands

Attila Berces[‡]

Steacie Institute for Molecular Sciences, National Research Council of Canada, Ottawa K1A 0R6, Canada

Received: October 17, 2000; In Final Form: November 30, 2000

The method of velocity map imaging is used to investigate the photoinduced dynamics of iodobenzene in weak laser fields as well as in fields of sufficient intensity to produce multiphoton excitation without dressing the potential energy surfaces. The speed and angular distributions of the recoiling iodine atoms observed with weak fields at 266 and 304 nm are in good agreement with previous studies, showing evidence of dissociation via n,σ* and π,π* states. Density functional theory calculations are used to determine the energies of the excited states. Ion and electron images produced with intense visible radiation (532−609 nm, 3×10^{10} to 5×10^{12} W/cm^2) show both two-photon threshold dissociation and higher order (four- to seven-photon) ionization processes. A unique characteristic of the I$^+$ images obtained with intense visible radiation is a continuous, hourglass-shaped feature peaked at zero kinetic energy, displaying highly nonstatistical speed and angular distributions. A mechanism that is consistent with all of the observations is dissociative autoionization of a superexcited repulsive Rydberg state.

I. Introduction

The competition between photoionization and photodissociation is inherently interesting because it is typically a multielectron and multicontinuum process.[1] In conventional studies with weak visible or ultraviolet radiation, a molecule absorbs a single photon and dissociates on the lowest potential energy surface accessible within the Franck−Condon window. For example, in synchrotron experiments an extreme ultraviolet photon excites a molecule, AB, to a neutral superexcited state, AB**, which can decay either by predissociation (to form A + B* or A$^+$ + B$^-$) or by autoionization (to form AB$^+$ + e$^-$). Dissociative ionization (to form A$^+$ + B + e$^-$) occurs if the ionic state is unbound.

Much more complex dynamics becomes possible with intense coherent radiation. Irradiation with visible or UV lasers at intensities sufficient to induce multiphoton absorption opens the possibilities of ladder switching and ladder climbing mecha-

nisms. Even though absorption of a single photon may be sufficient to dissociate the molecule, above-threshold absorption of additional photons[2] can lead to ionization and dissociation on higher potential energy surfaces. For polyatomic molecules, the competition between dissociation and above-threshold absorption opens the door to population of vibrational degrees of freedom that might not normally be accessible from the ground state. Still richer behavior becomes possible in fields strong enough to alter the potential energy that binds the molecule. In such strong fields, phenomena such as bond softening, stabilization, and field-induced tunneling become possible.[3]

In this study we have investigated the multiphoton dissociation and ionization of iodobenzene in an electromagnetic field of intermediate intensity. Alkyl and aryl iodides have been extensively studied as models of large molecules displaying complex photoinduced dynamics. The aryl iodides are especially interesting because of the presence of a second chromophore in the form of the aromatic π-electron system. The phenyl ring serves as an energy reservoir for the molecule, while funneling energy into the C−I reaction coordinate. The many potential energy surfaces generated by these two chromophores produce

Photodissociation and Photoionization of Iodobenzene

J. Phys. Chem. A, Vol. 105, No. 11, 2001 **2271**

multiple paths to higher energy dissociation and ionization channels, which compete with single-photon threshold dissociation.

Previous studies of the photodissociation of iodobenzene using weak nanosecond lasers, performed by the research groups of Bersohn,[4−6] El-Sayed,[7−13] Smalley,[14] and Leone,[15] revealed two distinct reaction mechanisms: a direct dissociation caused by excitation to an antibonding n,σ^* state and an indirect dissociation caused by a transition to a π,π^* state of the phenyl ring that is predissociated by the n,σ^* state. The former is analogous to the Q-manifold of HI and CH_3I, whereas the latter is analogous to the ^1L_b ($^1B_{2u} \leftarrow {}^1A_{1g}$) transition in benzene. These two transitions overlap in the weak A-band of iodobenzene, lying between 240 and 320 nm.[16] An analysis of the anisotropy of the recoiling fragments performed by El Sayed et al.,[10,12] and later confirmed by real-time measurements of Zewail et al.,[17,18] revealed that the direct, n,σ^* process occurs in less than a rotational period, whereas the indirect, π,π^* process occurs on the same time scale as rotation.

Multiphoton ionization of iodobenzene has been studied a number of times with both nanosecond[14,19] and shorter[20,21] pulses. The absence of the parent ion in any of the nanosecond studies was attributed to the very rapid predissociation of the S_1 state. Smalley et al.[14] placed an upper bound of 25 fs on the lifetime of this state, somewhat shorter than the later measurements of Zewail et al.[17,18]

In the present paper we investigate the effects of laser fields that are strong enough to induce multiphoton processes without altering the potential energy surfaces. A unique aspect of these experiments is our use of photofragment imaging,[22] which allows us to record both speed and angular distributions of a fragment in a single measurement. We find from these measurements that in the intermediate intensity regime fundamentally different reaction mechanisms, induced by above-threshold absorption (i.e., by absorption of additional photons above the lowest dissociation threshold), dominate the reaction dynamics. To compare these mechanisms with the previously observed threshold processes, we also performed a number of measurements with weak laser fields. In addition, to gain insight into the weak field processes, we performed density functional calculations on the low-lying electronic states of iodobenzene.

II. Methods

A. Experiments. We have used the velocity map imaging technique[22] to measure the speed and angular distributions of iodine ions and electrons. Experiments were performed with similar instruments located in Chicago, Kyoto, and Nijmegen.

In the Chicago laboratory, a linearly polarized laser pulse irradiated a molecular beam of iodobenzene seeded in 1 atm of He gas and pulsed at 10 Hz (General Valve). Various lasers were used in different wavelength regions: the second and fourth harmonics of a Nd:YAG laser (Continuum 681C, 10 ns) at 532 and 266 nm, respectively, a Nd:YAG-pumped dye laser (Continuum 681C/ Lambda Physik ScanMate II, 10 ns) at 304 (frequency doubled in a KDP crystal), 560, 570, 575, and 609 nm, and an excimer-pumped dye laser (Lambda Physik LPX 200/LPD 3000, 15 ns) at 266 nm (frequency doubled in a BBO crystal). The laser beams were focused with a 20 cm lens. The focal diameter of the Nd:YAG laser was measured with a scanning knife edge and was found to be $\gg 50$ mm. The intensity of the focused 532 nm radiation ranged from $\sim 3 \times 10^{10}$ to 5×10^{12} W/cm^2.

The molecular beam was pointed along the axis of a 71 cm long time-of-flight mass spectrometer. The skimmed molecular

beam source, the ionization chamber, and the flight tube were each differentially pumped. The laser was aligned perpendicular to the flight axis and focused onto the molecular beam between the repeller and extractor electrodes. Ions produced in this region were accelerated and focused onto a gated microchannel plate (MCP) assembly (Galileo 3040FM) mounted on the end of the flight tube. The electrode voltages were typically 2.61 kV for the repeller and 1.33 kV for the extractor.

Electrons produced on the MCP were accelerated by a 2.0 kV potential difference across the MCP onto a P47 phosphor screen. Mass discrimination was achieved by gating the potential on the front plate of the MCP from 0 to −500 V at the arrival time of the detected ion. The MCP anode voltage (applied to the phosphor) was 3.1 kV. The image produced on the phosphor screen was captured by a CCD camera (Sensoray SX11 frame grabber and COHO 4910 camera) and averaged in a laboratory computer. Typically, 20 000 laser shots were averaged to produce a two-dimensional map of the transverse recoil velocity of the gated ions. A slice of the full three-dimensional velocity distribution was generated by an inversion procedure developed by Matsumi et al.[23]

The Kyoto apparatus is similar to that in Chicago, except for a flight length of 60 cm and the use of 1 atm of Ar as a carrier gas. In some of the measurements a two-color pump-and-probe scheme, employing the fourth harmonic of a Nd:YAG laser (Quantel, Brilliant b) as the photolysis source and a Nd:YAG-pumped dye laser (Quantel, Brilliant b/Lambda Physik, Scan-Mate) as the probe, was utilized to eliminate nonresonant multiphoton ionization of the fragment I atoms.

The Nijmegen apparatus is similar to those in Kyoto and Chicago. Iodobenzene (5% in 1 atm of He) was expanded in a pulsed valve, skimmed, and passed along the time-of-flight axis of the imaging spectrometer. Both I^+ and photoelectron images were measured using a 37 cm time-of-flight tube. The 532 nm second harmonic output of a Nd:YAG laser (Spectra Physics GCR11) was used as the dissociation/ionization source. The electron images were acquired under exactly the same conditions as the I^+ images, except that the polarities of the repeller and extractor plates (2.00 and 1.44 kV, respectively) were reversed, and that the timing gate for the MCP voltage was moved closer ($\Delta t \approx 50$ ns) to overlap with the laser pulse to amplify selectively the electron signal.

Four sets of experiments were performed in the three laboratories: (i) Ion images were recorded in Chicago at 266 nm, using either the fourth harmonic of the Nd:YAG laser or a dye laser for both the pump and probe. In addition, two-color, pump-and-probe experiments were performed in Kyoto, using a 304 nm dye laser as the probe. (ii) Single-color ion images were recorded in Chicago at 304 nm using a dye laser. (iii) Single-color ion images were recorded in all three laboratories at 532 nm, using the second harmonic of the Nd:YAG laser over a range of intensities. Single-color images were also recorded in Chicago at longer (560−609 nm) wavelengths. (iv) Electron images were recorded in Nijmegen at 532 nm.

B. Density Functional Theory Calculations. Density functional theory (DFT) calculations were carried out in Ottawa, using the Amsterdam Density Functional program (version 2.3) derived from the work of Baerends et al.[24] and developed at the Free University of Amsterdam[25−27] and at the University of Calgary.[28] All optimized geometries calculated in this study are based on the local density approximation[29] augmented with gradient corrections to the exchange[30] and correlation[31] potentials. These calculations include quasi-relativistic corrections to the Hamiltonian introduced by Snijders et al.[32] Schreckenbach

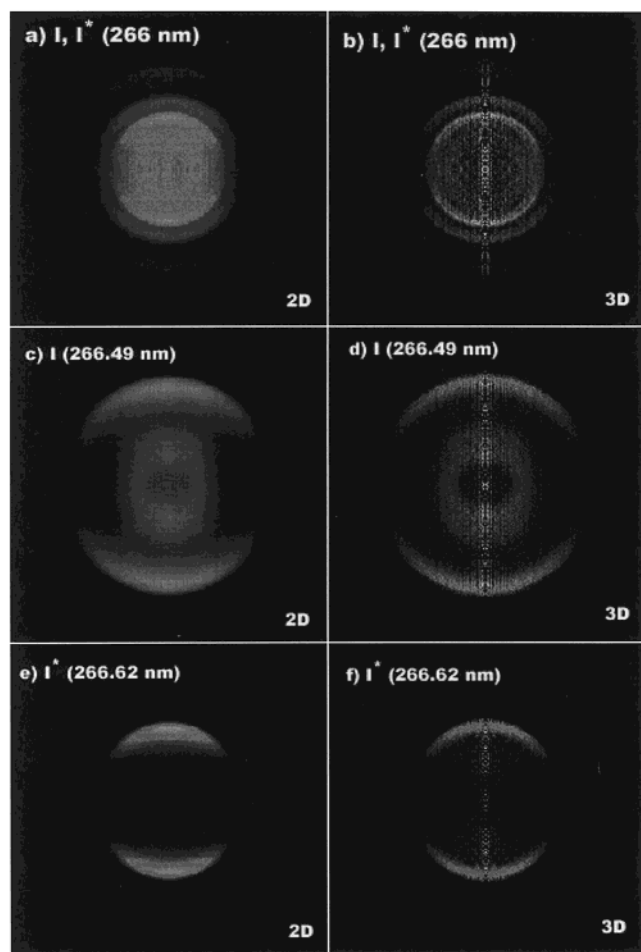**2272** *J. Phys. Chem. A, Vol. 105, No. 11, 2001*

Unny et al.

Figure 1. 2D symmetrized (left column) and 3D back-projected (right column) I$^+$ ion images obtained by single-color, 266 nm photodissociation of iodobenzene. Panels a and b were obtained using the fourth harmonic of a Nd:YAG laser. Panels c and d were obtained using a dye laser tuned to a (2 + 1) REMPI transition of I($^2P_{3/2}$). Panels e and f were obtained using a dye laser tuned to a (2 + 1) REMPI transition of I($^2P_{1/2}$). For these and all subsequent images, the polarization vector of the laser is vertical.
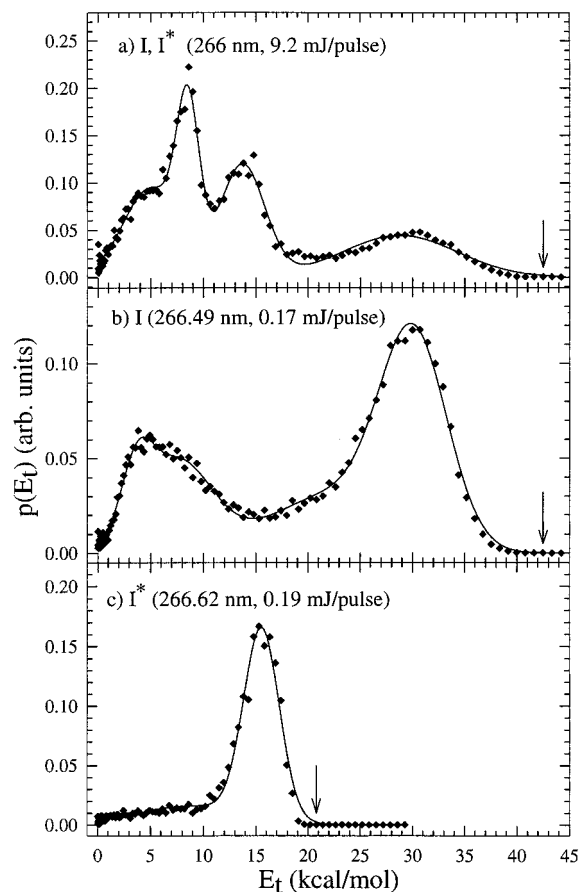

Figure 2. Kinetic energy distributions of the I$^+$ photofragment, extracted from the images in Figure 1. The smooth curves were obtained from a multi-Gaussian fit. The distributions correspond to photodissociation with (a) the fourth harmonic of a Nd:YAG laser and with a dye laser tuned to a (2 + 1) REMPI transition of (b) I($^2P_{3/2}$) and (c) I($^2P_{1/2}$). The arrows indicate the maximum kinetic energy available after dissociation by a single photon.

et al.[33] have implemented the analytic energy gradients of the quasi-relativistic corrections. All open shell calculations were spin unrestricted.

The atomic orbitals on iodine were described by an uncontracted triple-ζ Slater function basis set,[34] whereas a double-ζ Slater function basis set was used for carbon and hydrogen; a single-ζ polarization function was used on all atoms. The $1s^2$ configuration of carbon and the $1s^2 2s^2 2p^6 3s^2 3p^6 3d^{10} 4s^2 4p^6$ configuration of iodine were assigned to the core and treated by the frozen-core approximation.[24] The electron density was fitted to a set of s, p, d, f, g, and h Slater functions centered on all nuclei to calculate the Coulomb and exchange potentials accurately in each SCF cycle.[35]

III. Experimental Results

A. 266 nm. Single-color experiments were performed using the same laser to photodissociate iodobenzene and to ionize the iodine fragment. These experiments were performed with either the fourth harmonic of the Nd:YAG laser, which ionized both spin−orbit states of iodine nonresonantly, or the second harmonic of a dye laser tuned to detect either I($^2P_{3/2}$) or I($^2P_{1/2}$) by (2 + 1) resonance-enhanced multiphoton ionization (REMPI). The dye laser wavelengths were 265.97 and 266.49 nm for

I($^2P_{3/2}$) and 266.62 nm for I($^2P_{1/2}$). The nonresonant radiation obtained from the Nd:YAG laser had a pulse energy of 9.2 mJ, whereas the resonant, dye pulse energy was typically 0.1−0.3 mJ/pulse. Two-color experiments were also performed, using the fourth harmonic of the Nd:YAG laser to photodissociate the molecule and a dye laser tuned to 304.67 nm to ionize I($^2P_{3/2}$). The pulse energies of both lasers were typically 0.2 mJ.

The velocity map images of I$^+$ obtained in the one-color experiments are shown in Figure 1, and the corresponding center-of-mass relative kinetic energy distributions are plotted in Figure 2. Essentially equivalent results were obtained for I($^2P_{3/2}$) in the two-color experiments.

The images obtained with nonresonant radiation (Figure 1a,b) display three distinct rings (Figure 2a) peaked at 30.9, 14.9, and 8.7 kcal/mol. Additionally, there is a relatively broad shoulder near 4 kcal/mol. The kinetic energy distribution of the I($^2P_{3/2}$) fragments obtained with a dye laser (Figure 2b) shows two peaks, one at 30−31 kcal/mol (corresponding to the outermost ring in Figure 1d) and a second one at 3.4−4.9 kcal/mol. The latter peak is asymmetric and appears to have a shoulder near 8 kcal/mol. The I($^2P_{1/2}$) image has a single peak at 15.4 kcal/mol (Figure 2c).

A comparison of the kinetic energy distributions in Figure 2 shows a one-to-one correspondence between the structures seen in the nonresonant and resonant ion images. The shoulder near 4 kcal/mol and the peak at 30 kcal/mol in the nonresonant
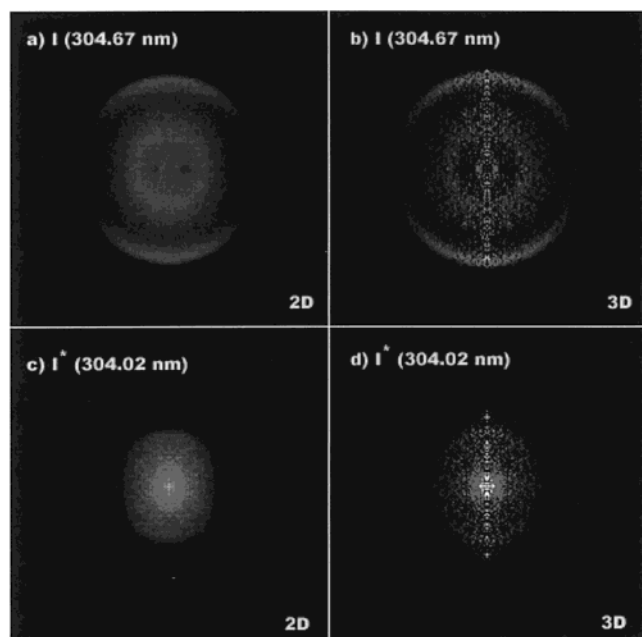
Photodissociation and Photoionization of Iodobenzene

J. Phys. Chem. A, Vol. 105, No. 11, 2001 **2273**

Figure 3. 2D symmetrized (left column) and 3D back-projected (right column) I^+ ion images obtained by single-color, 304 nm photodissociation of iodobenzene. Panels a and b were obtained using a dye laser tuned to a $(2 + 1)$ REMPI transition of $I(^2P_{3/2})$. Panels c and d were obtained using a dye laser tuned to a $(2 + 1)$ REMPI transition of $I(^2P_{1/2})$.

spectrum (panel a) correspond to the two maxima in the $I(^2P_{3/2})$ distribution panel (b), whereas the peak at 14.9 kcal/mol matches that at 15.4 kcal/mol in the $I(^2P_{1/2})$ distribution (panel c). The sharp peak at 8.7 kcal/mol in the nonresonant spectrum is located at the same energy as the broad shoulder in the $I(^2P_{3/2})$ distribution.

The locations of the peaks in the $I(^2P_{3/2})$ spectrum are in good agreement with the time-of-flight spectra of Freitas et al.[9] The features that we observe at 4 and 8.7 kcal/mol are not resolved, however, in the latter data. No studies of $I(^2P_{1/2})$ at this excitation energy have been reported previously.

The anisotropy parameters β_2 and β_4

$$p(\theta) = 1 + \beta_2 P_2(\cos\theta) + \beta_4 P_4(\cos\theta) \qquad (1)$$

defined by the Legendre series were obtained by a least-squares fit to the angular distributions of the images. The fitted values of β_2 for $I(^2P_{3/2})$ are in reasonable agreement with those reported by Freitas et al.[9] For the 15.4 kcal/mol peak in the $I(^2P_{1/2})$ spectrum we obtained values of $\beta_2 = 2.8 \pm 0.2$ and $\beta_4 = 0.7 \pm 0.1$. For the corresponding peak at 14.9 kcal/mol in the Nd: YAG spectrum the anisotropy parameters were $\beta_2 = 0.8 \pm 0.1$ and $\beta_4 = -0.4 \pm 0.1$.

B. 304 nm. Single-color experiments were performed using a tunable dye laser to detect $I(^2P_{3/2})$ at 304.67 nm and $I(^2P_{1/2})$ at 304.02 nm. The images and kinetic energy distributions are shown in Figures 3 and 4, respectively. The maximum at 23 kcal/mol and the broad feature between 5 and 10 kcal/mol in the $I(^2P_{3/2})$ spectrum correspond to the peaks reported by Hwang and El-Sayed[7] at 24.8 and 10.2 kcal/mol, and the maximum for $I(^2P_{1/2})$ near 7 kcal/mol corresponds to their peak at 5.7 kcal/mol.

C. 532 nm. The velocity map images of I^+ produced by irradiating iodobenzene at 532 nm in all three laboratories show two types of features: one or more discrete rings and an intense central feature that has a continuous "hourglass" shape. These features are readily evident in the image shown in Figure 5.
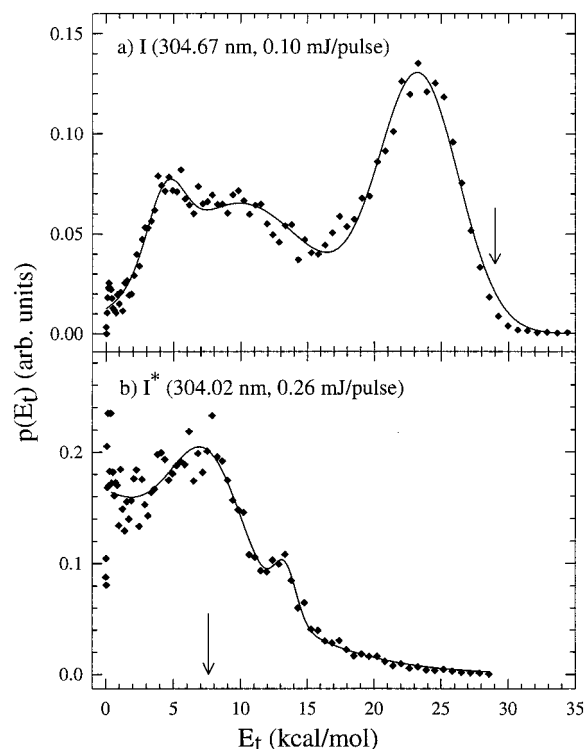

Figure 4. Kinetic energy distributions of the I^+ photofragment, extracted from the images in Figure 3. The smooth curves were obtained from a multi-Gaussian fit. The distributions correspond to photodissociation with a dye laser tuned to a $(2 + 1)$ REMPI transition of (a) $I(^2P_{3/2})$ and (b) $I(^2P_{1/2})$. The arrows indicate the maximum available kinetic energy for dissociation by a single photon.

The corresponding kinetic energy distribution, shown in Figure 6a, displays (i) a broad peak at 30 kcal/mol, (ii) a sharp peak at 14 kcal/mol, (iii) a shoulder at 8 kcal/mol, and (iv) a sharp maximum at zero energy. The first three features correspond to a similar structure found in the 266 nm distributions, whereas the last corresponds to the hourglass seen only at the visible wavelengths. The ratio of the integrated signal produced by the hourglass to that produced by the outer ring was found to increase slowly with laser intensity.

The angular distributions of these features are shown in Figure 7. The smooth curves are least-squares fits of the Legendre series in eq 1. The fitted anisotropy parameters are listed in Table 1. In the case of the hourglass feature, β_2 was found to increase monotonically with recoil energy, as shown in Figure 8. The qualitative shape of the hourglass feature was insensitive to laser intensity for pulse energies ranging from 6.4 to 108 mJ. Closer inspection, however, reveals that β_2 increases more slowly at higher laser intensity, as shown in Figure 8.

In Figure 9 is displayed an electron image that was recorded under the same experimental conditions as the ion image in Figure 5. The corresponding kinetic energy distribution in Figure 6b shows two peaks riding on top of a continuous background. Possible assignments of the ion and electron peaks are discussed in section V.

D. 560−609 nm. The variation of the image properties with wavelength is shown in Figures 10 and 11. At longer wavelengths the hourglass feature completely dominates the image. In Figure 10a only the outermost ring is observed. The absence of the inner ring and shoulder at 532 nm in the Chicago and Kyoto data is surprising. It is possibly caused by lower energy resolution, or perhaps by differences in laser mode structure that affect the relative intensities of competing multiphoton processes, which are discussed in section V.
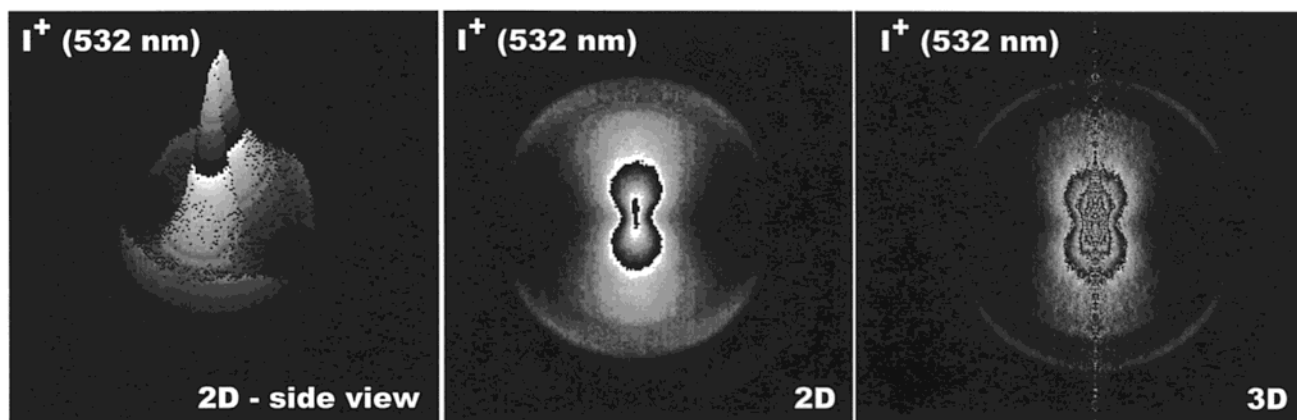
Figure 5. 2D symmetrized (left and center panels) and 3D back-projected (right panel) I⁺ ion images obtained by photodissociation of iodobenzene at 532 nm.

TABLE 1: Ion and Electron Anisotropies at 532 nm

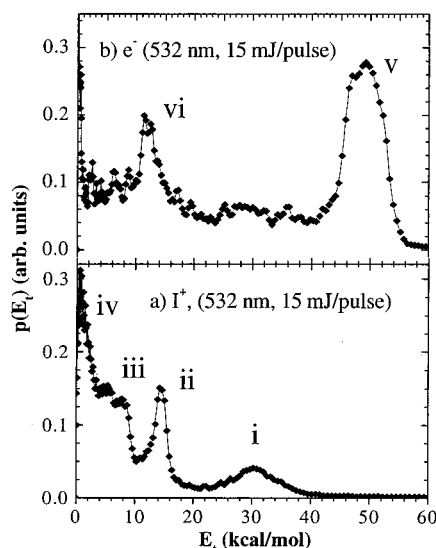| peak number[a]	i	ii	iii	iv	v	vi
kinetic energy (kcal/mol)	30	14	8	1	48	12
detected species	I⁺ ion	I⁺ ion	I⁺ ion	I⁺ ion	electron	electron
β_2	1.30 ± 0.06	1.16 ± 0.04	1.77 ± 0.04	1.00 ± 0.01	1.7 ± 0.2	0.8 ± 0.2
β_4	0.63 ± 0.05	0.86 ± 0.03	0.58 ± 0.03		1.5 ± 0.2	0.9 ± 0.2

[a] Peak numbers correspond to those in Figures 6 and 7.

Figure 6. Kinetic energy distributions of the (a) I⁺ photofragments and (b) photoelectrons obtained by excitation of iodobenzene at 532 nm.
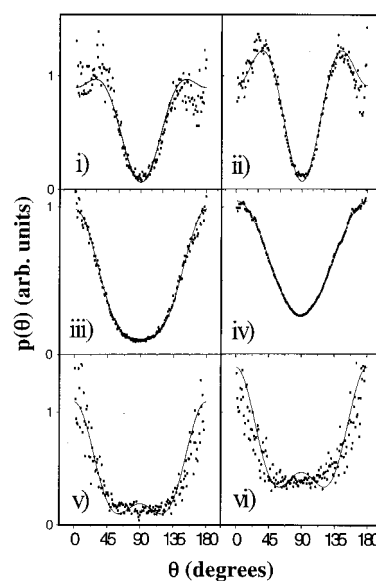

Figure 7. Angular distributions of ions and electrons obtained by excitation of iodobenzene at 532 nm. The numerals in the various panels correspond to the features labeled in Figure 6. The smooth curves are least-squares fits of eq 1.

IV. Potential Energy Calculations

The results of the density functional theory calculations are summarized in Figure 12 and Table 2. Shown in Figure 12 are the highest occupied and lowest unoccupied orbitals of iodobenzene, along with the corresponding orbitals of benzene with which they are correlated. The occupied $2A_2$, $7B_2$, and $4B_1$ orbitals have π, n, and π character, respectively, whereas the unoccupied $11A_1$, $3A_2$, and $5B_1$ orbitals have σ^*, π^*, and π^* character. Listed in Figure 12 are the orbital energies determined by the DFT calculations. In Table 2 are listed both the vertical and minimum excitation energies for the 10 lowest transitions. The differences between the singlet and triplet energies are only lower bounds because of spin contamination of the orbitals.

V. Discussion

A. Overview. We start the discussion in section V.B with an analysis of the discrete structure observed at 266, 304, and

532 nm. These results are in general agreement with previous weak field measurements and with the DFT calculations. We then go on in section V.C to discuss the hourglass feature observed at 532 nm and longer wavelengths. This feature is the main new result of this paper and involves a qualitatively new reaction mechanism, which we believe has not been previously reported. We conclude in section V.D with a discussion of the electron image, which provides a test of the proposed mechanism.

B. Discrete Structure. The anisotropy of the outermost ring in Figure 1a,c shows that the highest energy peak in the C_6H_5 + I($^2P_{3/2}$) channel at 266 nm is produced by a parallel electronic transition. Previous studies by the groups of Bersohn, El-Sayed, and Zewail identified the mechanism of the high-energy product to be promotion of a nonbonding electron to an antibonding
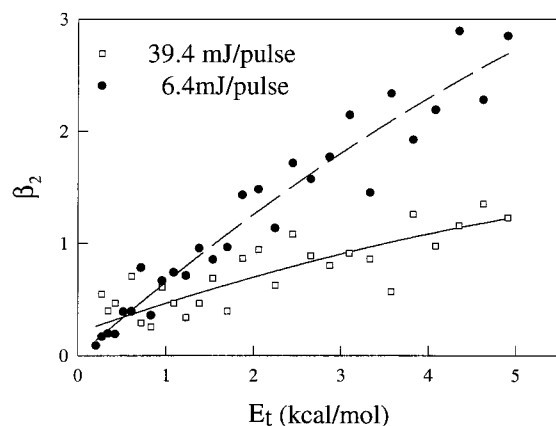
Photodissociation and Photoionization of Iodobenzene

J. Phys. Chem. A, Vol. 105, No. 11, 2001 **2275**

Figure 8. Variation of the anisotropy parameter β_2 with the center of mass recoil energy of iodobenzene at 532 nm. Open and closed symbols refer to laser pulse energies of 39.4 and 6.4 mJ, respectively.

TABLE 2: Density Functional Theory Calculations

transition	excited state	vertical energy (eV)	minimum energy (eV)
(a) $4B_1 \rightarrow 11A_1$	$^3B_1$	3.810	3.089
	$^1B_1$	3.946	3.178
(b) $4B_1 \rightarrow 3A_2$	$^3B_2$	4.488	4.323
	$^1B_2$	4.649	4.467
(c) $4B_1 \rightarrow 5B_1$	$^3A_{13}$	4.109	3.606
(d) $7B_2 \rightarrow 11A_1$	$^3B_{22}$	4.438	3.011
	$^1B_{22}$	4.616	
(e) $7B_2 \rightarrow 3A_2$	$^1B_{12}$	6.195	
	$^3B_{12}$	6.162	
(f) $7B_2 \rightarrow 5B_1$	$^1A_2$	6.106	5.809
	$^3A_2$	6.094	5.787
(g) $2A_2 \rightarrow 11A_1$	$^1A_{22}$	5.560	4.604
	$^3A_{22}$	5.555	4.604
(h) $2A_2 \rightarrow 3A_2$	$^3A_{12}$	4.350	3.833
(i) $2A_2 \rightarrow 5B_1$	$^1B_{13}$	5.173	
	$^3B_{13}$	4.938	
(j) $10A_1 \rightarrow 11A_1$	$^3A_{11}$	5.927	3.723

orbital by a parallel transition[38]

$$n^2 + h\nu \rightarrow {}^3Q_0(n,\sigma^*) \rightarrow C_6H_5 + I(^2P_{3/2}) \qquad (2)$$
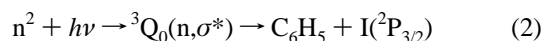
The photoexcitation step in this mechanism corresponds to process d in the DFT calculation. The predicted vertical excitation energy for this transition is 102 kcal/mol, which is accessible with a single photon at 266 nm.

The maximum energy available for translation is given by[9]

$$E_{avl} = h\nu - D_0^{\,0} + E_{int}^{\,p} \qquad (3)$$

where $D_0^{\,0}$ is the C−I bond dissociation energy at 0 K and $E_{int}^{\,p}$ is the internal energy of the parent molecule. Taking $D_0^{\,0} = 66.7 \pm 0.7$ kcal/mol[37] and $E_{int}^{\,p} = 2.0$ kcal/mol at 298 K,[38] the available energy for $I(^2P_{3/2})$ at 266.49 nm is 42.5 kcal/mol. The maximum translational energy of $I(^2P_{3/2})$ in Figure 2a,b is just below this value. The translational energy at the peak, E_{peak}, is 30 kcal/mol, which is 71% of E_{avl}. The modification of Trentelman et al.[39] of the impulsive model of Busch and Wilson[40] predicts a maximum relative translational energy of only 23% of E_{avl}. The much larger observed value of E_{peak} suggests that the geometry of the aromatic carbon atoms is not well suited for converting the recoil energy into vibrational modes of the phenyl ring. In any event, the very large recoil energies support the assignment of the outer peak to a direct, $n\sigma^*$ transition. It is very likely that the same mechanism applies to the outermost ring in the 532 nm images, except that two photons of the same total energy must be absorbed.

It is tempting to assign the mechanism[36]

$$n^2 + h\nu \rightarrow {}^3Q_0(n,\sigma^*) \rightarrow C_6H_5 + I(^2P_{1/2}) \qquad (4)$$
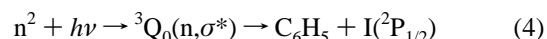
to the production of $I(^2P_{1/2})$ in Figure 1e, for which the maximum recoil energy is just below E_{avl} (see Figure 2c). A difficulty with this assignment, however, is that the values of $\beta_2 > 2$ and $\beta_4 \neq 0$ observed with the dye laser indicate the absorption of more than one photon. The smaller value of β_2 observed with the much more intense Nd:YAG laser (Figure 1a) and the slight shift in E_{peak} (Figure 2a) suggest that overlapping transitions may be involved. The absence of a peak at 14 kcal/mol in the 532 nm images recorded in Chicago and Kyoto suggests that it may be produced by a higher order multiphoton process than that which produces the hourglass feature. We note that Zhang et al.[41] reported evidence from time-of-flight spectra of significant contributions from multiphoton processes to the dissociation of iodobenzene at 266 nm. Further experimental work is needed to clarify this point.

Freitas et al.[9] have assigned the same mechanism for the high-energy peak at 304 nm as at 266 nm. Although we find in Figure 4a that the maximum recoil energy slightly exceeds E_{avl}, the excess energy lies within the uncertainty of $D_0^{\,0}$.[42] For $I(^2P_{1/2})$, however, it is quite clear that more than one photon must be
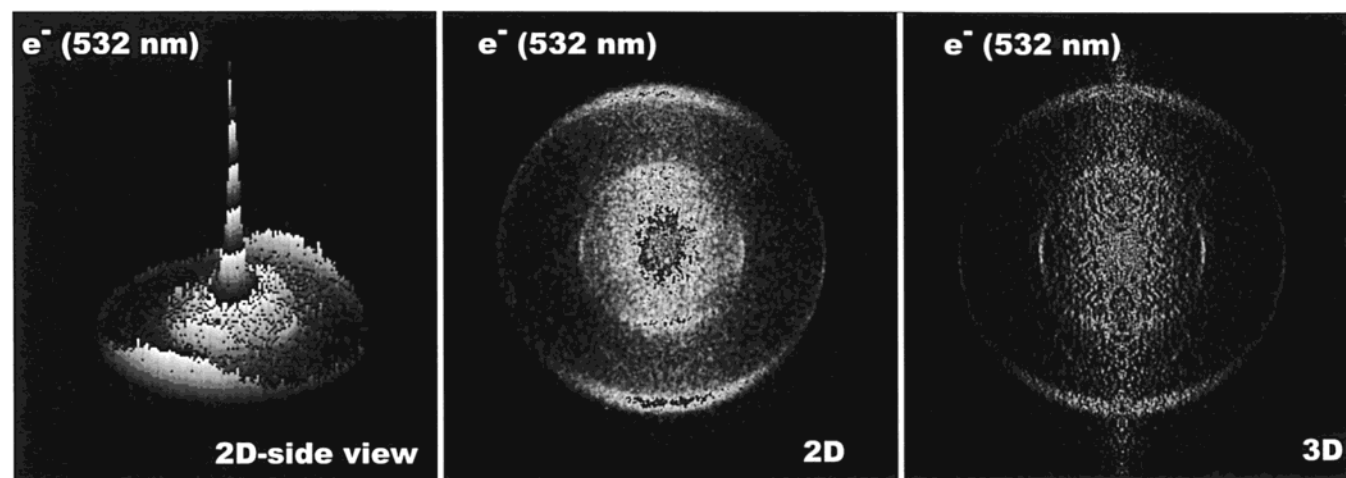

Figure 9. 2D symmetrized (left and center panels) and 3D back-projected (right panel) photoelectron images of iodobenzene at 532 nm.
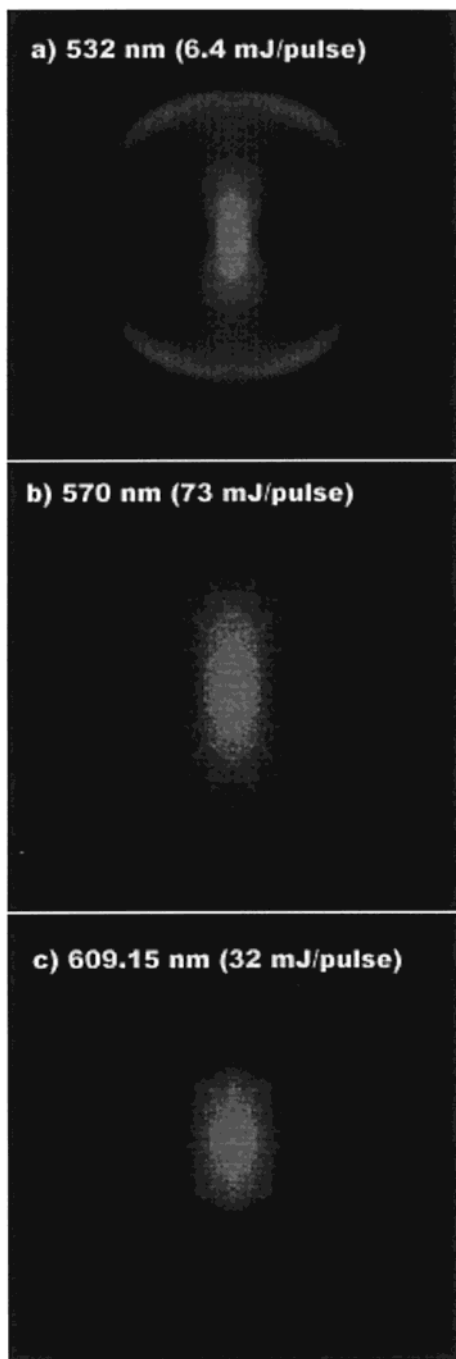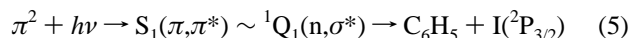
Figure 10. Wavelength study of the 2D symmetrized I^+ ion images of iodobenzene at (a) 532 nm, (b) 570 nm, and (c) 609.15 nm.

Figure 11. Wavelength study of the kinetic energy distributions of the I^+ photofragment of iodobenzene at (a) 532 nm, (b) 560 nm, (c) 570 nm, (d) 575 nm, and (e) 609.15 nm. The curves are a phase space calculation of the center-of-mass kinetic energy distribution for two-photon photodissociation of the neutral molecule, normalized to the data at 1.5 kcal/mol.

absorbed to account for the outermost peak, and probably also for the lower energy peak.

The low-energy peaks at 266 and 304 nm (appearing at 4 kcal/mol in our data) have been assigned by El-Sayed and co-workers[7,11] to a mechanism involving the excitation of a phenyl π-orbital followed by intersystem crossing to the $n\sigma^*$ surface

$$\pi^2 + h\nu \rightarrow S_1(\pi,\pi^*) \sim {}^1Q_1(n,\sigma^*) \rightarrow C_6H_5 + I({}^2P_{3/2}) \quad (5)$$

where $\sim$ designates a radiationless transition. The lowest transition of this type is process b in the DFT calculations. The predicted vertical transition energy is $103.5-107.2$ kcal/mol, which corresponds closely to the photon energy at 266 nm. Vibrational excitation of the phenyl ring is expected for such a vertical transition because of the increased equilibrium distance
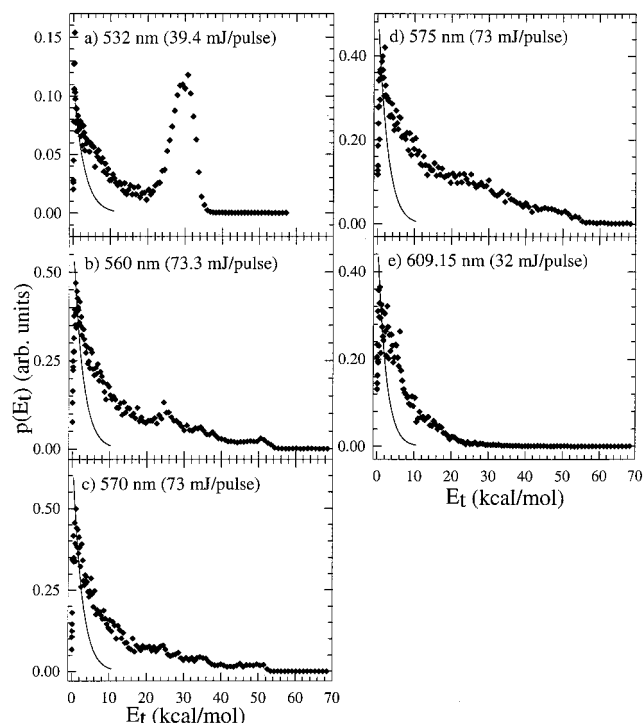
of the C–I bond in the S_1 state. The poor coupling between the phenyl modes and the C–I stretch mentioned previously for $n\sigma^*$ excitation could also explain the small recoil energy and small angular anisotropy for $\pi\pi^*$ excitation. This conclusion is consistent with the finding of Zewail et al.[17,18] that the low-energy product recoils on the same time scale as the rotational period.

The shoulder observed near 8 kcal/mol in the 266 nm dye laser distribution, along with the corresponding maximum at 8.7 kcal/mol in the 266 Nd:YAG data and the shoulder in the 532 nm data, is more difficult to assign. One possibility is that the double features seen at 4 and 8 kcal/mol are produced by singlet/triplet splitting of the S_1 state. But the marked variation in relative intensities in the various spectra and the absence of the 8.7 kcal/mol peak in the two-color pump-and-probe images suggest that this feature may be produced by a multiphoton process.

C. Hourglass Feature. The hourglass feature seen in the 532 nm images is the most striking aspect of this work, and indeed it has motivated this study. Great care was taken to rule out possible artifacts that might have produced this effect. Analysis with a gas chromatograph/mass spectrometer did not reveal any impurities that might have produced the hourglass. Addition of HI to the molecular beam demonstrated that parent HI^+ or its I^+ fragment was not present under normal conditions. Likewise, we ruled out the possibility that the parent iodobenzene ion might have "leaked through" the mass gate.

For the photofragments to recoil very slowly, there must be some sink for the available energy. One possibility is a van der Waals cluster, which is known to dissociate with a broad velocity distribution peaked near zero kinetic energy.[43,44] We ruled out this many-body mechanism by demonstrating that the shape of the image is unaffected by variation of the time delay between the nozzle and laser pulses or by changes in the pressure
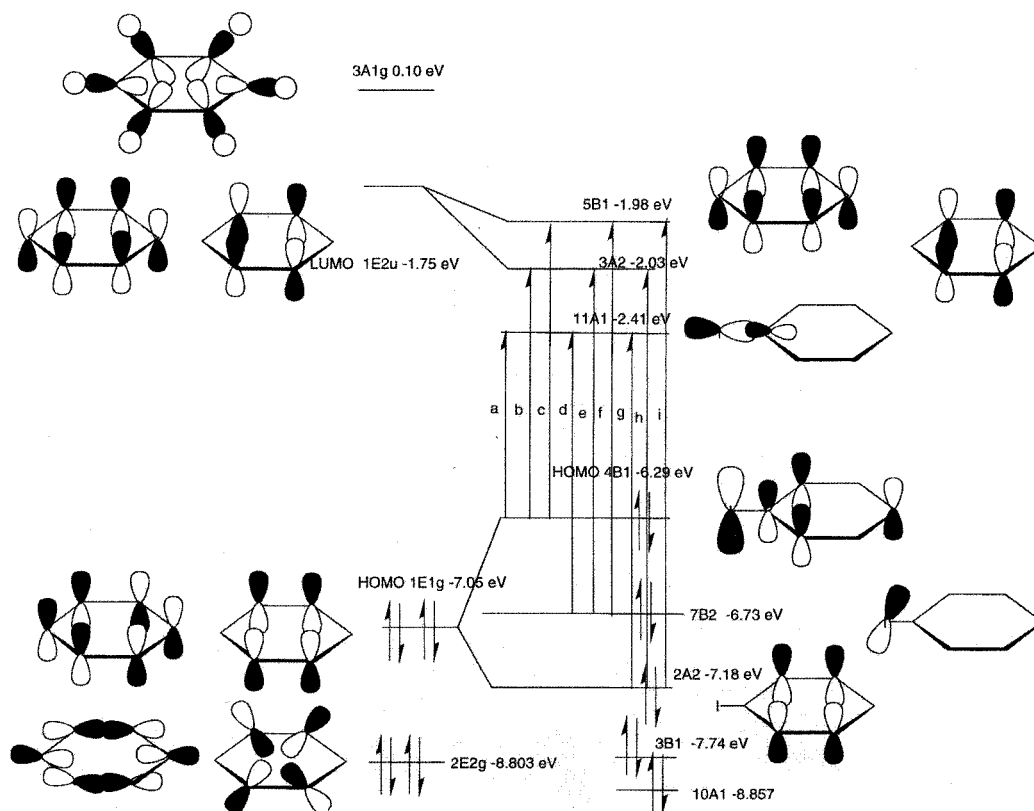
Photodissociation and Photoionization of Iodobenzene

J. Phys. Chem. A, Vol. 105, No. 11, 2001 **2277**

Figure 12. Molecular orbital diagram depicting the energetics of the allowed HOMO−LUMO transitions in benzene (left) and iodobenzene (right). The orbital energies were calculated by density functional theory.

and composition of the carrier gas. Moreover, it would be difficult to understand why cluster effects are present at 532 nm and absent at 266 nm.

Another class of mechanisms that we considered is that of field-induced effects. Broad, anisotropic images, which have been observed in the high-intensity ($\sim 10^{13}$ W/cm^2) photoionization and photodissociation of H$_2$, were attributed to dressed-state effects such as field-enhanced avoided crossings.[45] Such mechanisms are unlikely to be operative in the present case because the intensity was generally much lower and, more importantly, because the shape of the hourglass was only weakly dependent on the intensity. Another field-induced effect that we considered is alignment of the molecule by the electric field of the laser.[46] Although dynamical alignment may contribute to the shape of the image, the insensitivity of the image to intensity or expansion conditions argues against this process as the primary mechanism.

A possible sink for the available energy is the bath of vibrational states provided by the phenyl ring. A statistical distribution of the internal energy among all vibrational degrees of freedom predicts a most probable recoil energy very close to zero.[47] For such a mechanism to explain the data, it is necessary to account for the lack of an hourglass at shorter wavelengths. A possible explanation is that the repulsive $n\sigma^*$ surface acts as a springboard for *above-threshold absorption* of additional photons, as depicted schematically in Figure 13b. The probability of enhanced absorption should be sensitive to wavelength, and in the case of iodobenzene one might argue that this effect is greater for lower energy photons. As the molecule begins to dissociate, different vibrational modes of the upper surface enter the Franck−Condon window, leading thereby to the population of additional degrees of freedom. Such an effect has in fact been detected in electron images of CH$_3$I excited at 248 nm.[48]

Further thought shows that both the angular and speed distributions are incompatible with a statistical mechanism. The marked directionality of the hourglass is inconsistent with a long-lived complex. Moreover, one would expect that an ensemble of molecules that decays stochastically would have an anisotropy that is independent of recoil speed, inasmuch as the partitioning of energy between internal and external degrees of freedom should be independent of survival time. That is to say, the ratio of slow to fast fragments should be the same in every time interval. Experimentally, however, we find that β_2 increases with recoil energy (Figure 8). We tested the statistical hypothesis further by using phase space theory[49,50] to calculate the kinetic energy distribution as a function of available energy. The resulting distributions, plotted in Figure 11 for different wavelengths, fall off much more rapidly than observed.

A related mechanism is multiphoton ionization of the molecule, followed by photodissociation of the parent ion. A large body of literature[51] has shown that the photodissociation of aromatic molecular ions produces a statistical kinetic energy distribution, peaked near zero. A phase space theory calculation assuming the same vibrational frequencies for the ion as the molecule, but with a dissociation energy of 53.8 kcal/mol,[52] again predicts a kinetic energy distribution that is much steeper than observed.[53]

An interesting variation of the mechanism depicted in Figure 13b is based on the observation[54] that the energy of the 532 nm photon corresponds almost exactly to the $\nu = 7$ overtone of the C−H stretch.[55] Absorption of additional photons by molecules in this highly excited state could conceivably populate a unique set of states that produce the hourglass recoil distribution. This proposal is ruled out, however, by the observation in Figures 10 and 11 that the hourglass is present at wavelengths that do not correspond to C−H overtone transitions. The dependence of the shape of the central feature
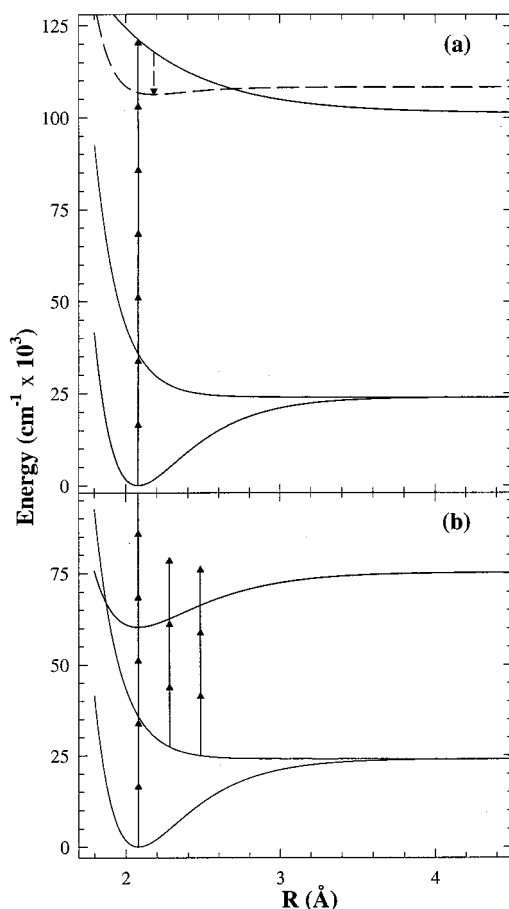
Figure 13. Schematic drawings illustrating the competition between (a) autoionization and dissociation of a superexcited state and (b) dissociation and above-threshold absorption by a valence state. The potential energy curves are all hypothetical. The solid curves correspond to neutral states, and the dashed curve corresponds to an ionic state. The solid arrows indicate photon absorption, whereas the dashed arrow depicts emission of an electron. In mechanism a, the electron carries away a continuous amount of kinetic energy, so that the recoiling ion—neutral pair have a kinetic energy peaked near zero. In mechanism b, the absorption of more than two photons populates an excited electronic state. The competition between dissociation and absorption allows a variety of vibrational modes to be excited.

on wavelength does suggest, however, that Franck—Condon overlap plays an important role.

Having ruled out both internal and external energy sinks as well as collisions with another (loosely bound or free) molecule, we are left with a three-body fragmentation as the only viable mechanism for explaining the zero kinetic energy peak. The mechanism that we propose is multiphoton *dissociative ionization* (DI), with the rapidly departing electron removing most of the available energy. This mechanism is depicted schematically in Figure 13a. In this mechanism, the molecule absorbs six or seven photons to reach a doubly excited, neutral Rydberg state. The superexcited electronic configuration includes an antibonding electron that causes nuclear repulsion and a Rydberg electron that lies above the ionization threshold. The molecule can either dissociate on the neutral potential energy surface or autoionize to a repulsive ionic surface. We suppose further that the ionic surface is much less repulsive than the neutral one. If the molecule autoionizes promptly, the electron carries away most of the available energy and the nuclear fragments recoil slowly, whereas if the molecule survives for a long time before autoionizing, the nuclear fragments acquire a larger fraction of the available energy while still on the neutral surface. The

translational energy distribution is peaked near zero because the probability of autoionization per unit time is greatest near the turning point of the trajectory. Like some of the other processes that we considered, this mechanism also depends on an intermediate state to project out a specific class of excited states (in this case an antibonding Rydberg state). The observed intensity dependence of the hourglass feature is consistent with an above-threshold mechanism. A quantitative assessment of the intensity dependence of the branching ratio is difficult, however, because the same laser pulse was used both to excite the molecule and to ionize the iodine fragment. The latter is a six-photon nonresonant process. Above-threshold excitation of iodobenzene, on the other hand, is very likely to involve one or more resonances at higher energy. At the intensities required to ionize the I atom, above-threshold excitation of iodobenzene is therefore likely to be strongly saturated.

How realistic is the DI mechanism? In a closely related study, Unny et al.[56] observed both discrete and continuous structure in the velocity map images of I^+ produced by visible multiphoton excitation of I_2, with a maximum at zero kinetic energy. In the absence of collisions and dressed-state effects, such continuous structure for a diatomic molecule could be caused *only* if a third body (i.e., an electron) carries away the excess energy. They also observed an hourglass feature in the 532 nm photoexcitation of CH_3I.[57] In weak-field, synchrotron studies of the DI of H_2, a structured kinetic energy distribution was observed with a peak at zero energy.[58] For this molecule the doubly excited states have been identified as the Q_1 and Q_2 Rydberg states,[59] and the zero kinetic peak has been attributed to the DI mechanism. Multiphoton dissociative ionization taking place after (2 + 1) REMPI of H_2 via the E,F double-well state has been studied in detail by Bakker et al.[60] using velocity map imaging. Multiphoton DI of NO_2 has been detected by Hayden and co-workers[61] in electron—ion coincidence measurements. These experiments suggest that DI may be a fairly common mechanism for the decay of small, highly excited molecules. Although for large molecules it is possible that the large density of states of the polyatomic fragment may play some role in partitioning the energy, DI is the only mechanism that we have found that can account for all of the qualitative properties of the data.

The role played by the repulsive intermediate state continues to be an interesting question. Our experiments provide strong evidence that, contrary to previous conclusions,[16-18] the iodobenzene molecule may be ionized with nanosecond laser pulses. We speculate that the "launching pad" provided by this state facilitates the excitation of a second electron, which is required to produce the doubly excited Rydberg state. Prompt dissociation (or photodissociation) of the superexcited state prevents observation of the parent ion. It would be very interesting to repeat these experiments with synchrotron radiation to see if the hourglass effect is produced with weak-field, single-photon excitation.

What produces the anisotropy of the hourglass? The angular distribution is likely to be caused by a combination of the excitation and decay processes. In the axial recoil limit, a sequence of *m* parallel and *n* perpendicular transitions produces an angular distribution[62] that varies as $\cos^{2m}\theta \sin^{2n}\theta$. For $m > n$ the distribution is aligned along the electric vector of the laser. In the dissociation process, molecules that recoil very slowly lose some of their anisotropy. (In the classical limit[62] for a single photon, β_2 is reduced by a factor of 4.) According to the DI model, the rapid fragments come from molecules that dissociate promptly on the neutral surface, whereas the slow fragments

Photodissociation and Photoionization of Iodobenzene

J. Phys. Chem. A, Vol. 105, No. 11, 2001 **2279**

TABLE 3: Mechanisms for Electron Production

mechanism[a]	no. of photons	electron energy at 532 nm (kcal/mol)
dissociation		
PhI → Ph + I, I*	2	
(1a) Ph → Ph$^+$	4	28
(1b) I → I$^+$	5	27.5
(1c) I* → I$^+$	5	49.3
ionization		
(2) PhI → PhI$^+$	4	14
dissociative ionization		
(3a) PhI → Ph$^+$ + I	5	15
(3b) PhI → Ph + I$^+$	6 or 7[b]	15

[a] I and I* denote I($^2P_{3/2}$) and I($^2P_{1/2}$), respectively. [b] For wavelengths greater than 563 nm.

originate from ions that take much longer to dissociate. Consequently, β_2 is expected to increase monotonically with recoil energy, as observed.

D. Electron Images. Velocity distributions of the electrons can be useful for identifying the photoionization mechanism. There are three possible sources of electrons: (1) photodissociation of iodobenzene into neutral fragments, followed by post-ionization of either the I atom or the phenyl radical, (2) ionization of the parent molecule, and (3) dissociative ionization to produce either iodine or phenyl ions. The energetics of these multiphoton processes are listed in Table 3, which should be compared with the kinetic energy distributions shown in Figure 6b. By accident, the energies available to the electron in several of these processes are indistinguishable. For example, the maximum energy available in the ionization of phenyl by four photons is 28 kcal/mol, whereas the energy available in the ionization of I($^2P_{3/2}$) by five photons is 27.5 kcal. Similarly, both mechanisms 2 and 3 release 14−15 kcal/mol. These coincidences could be avoided by using a different photon energy.

The high-energy peak in the electron image corresponds to the ionization of I($^2P_{1/2}$) (mechanism 1c). The ionization of I($^2P_{3/2}$) and C_6H_5 produces a broad, weak feature near 28 kcal/mol. The inner peak near 12 kcal/mol could be explained by either ionization of the parent molecule or by DI, with several kilocalories per mole of available energy appearing as a vibration. In either case, this peak is conclusive evidence of above-threshold ionization of the molecule. The angular distributions of the peaks at 12 and 48 kcal/mol have pronounced β_4 values (Table 1) that show the multiphoton nature (i.e., from combined parallel and perpendicular transitions) of the excitation and dissociation processes.

The electron image also contains a sharp, narrow peak at zero kinetic energy with a broad high-energy tail (Figures 6b and 9). The peak at zero kinetic energy could be caused by direct excitation to a repulsive ionic potential energy surface, whereas the tail might have contributions from a DI mechanism. The broad tail distorts the relative intensities and angular distributions of the weaker peaks at higher energy. In conclusion, we find that the electron image is consistent with, but does not confirm, the DI mechanism. Further work, probably at wavelengths >600 nm, is required.

VI. Conclusions

We have used the method of velocity map imaging to explore the photodissociation and photoionization dynamics of iodobenzene at low (∼10^9 W/cm^2) and intermediate (∼3 × 10^{10} to 5 × 10^{12} W/cm^2) laser intensities. In weak fields we observed photodissociation products attributed to nσ^* and π,π^* channels,

in good agreement with our density functional theory calculations and with previous time-of-flight measurements. Qualitatively new behavior was observed in fields strong enough to produce multiphoton excitation without inducing tunneling effects. The signature of this behavior is a continuous, hourglass-shaped feature peaked at zero kinetic energy, which was observed at wavelengths between 532 and 609 nm.

The production of low-energy neutral and/or ionic fragments requires the existence of a sink for most of the energy absorbed from the field. The highly nonstatistical energy and angular distribution of the fragments rule out the possibility that the vibrational states of the phenyl ring fulfill that role. A mechanism that explains all of the data is three-body dissociative ionization, in which the electron carries off most of the kinetic energy. Contrary to reports of previous studies, we find that multiphoton ionization of the parent molecule competes effectively with two-photon threshold dissociation and predissociation. An electron image confirmed the occurrence of multiphoton ionization, but did not by itself conclusively establish the three-body dissociative ionization mechanism.

References and Notes

(1) Nenner, I.; Beswick, J. A. In *Handbook of Synchrotron Radiation*; Marr, G. V., Ed.; Elsevier: Amsterdam, 1987; Vol. 2, pp 355−466.

(2) Magnier, M.; Persica, M.; Rahman, M. *J. Phys. Chem. A* **1999**, *103*, 10691.

(3) Levis, R. J.; DeWitt, M. J. *J. Phys. Chem. A* **1999**, *103*, 6493.

(4) Dzvonik, M.; Yang, S.; Bersohn, R. *J. Chem. Phys.* **1974**, *61*, 4408.

(5) Kawasaki, M.; Lee, S. J.; Bersohn, R. *J. Chem. Phys.* **1977**, *66*, 2647.

(6) Freedman, A.; Yang, S. C.; Kawasaki, M.; Bersohn, R. *J. Chem. Phys.* **1980**, *72*, 1028.

(7) Hwang, H. J.; El-Sayed, M. A. *J. Photochem. Photobiol., A* **1996**, *102*, 13.

(8) Griffiths, J. A.; Jung, K.; El-Sayed, M. A. *J. Phys. Chem.* **1996**, *100*, 7989.

(9) Freitas, J. E.; Hwang, H. J.; El-Sayed, M. A. *J. Phys. Chem.* **1995**, *99*, 7395.

(10) Hwang, H. J.; Griffiths, J. A.; El-Sayed, M. A. *Int. J. Mass Spectrom. Ion Processes* **1994**, *131*, 265.

(11) Freitas, J. E.; Hwang, H. J.; El-Sayed, M. A. *J. Phys. Chem.* **1993**, *97*, 12481.

(12) Hwang, H. J.; El-Sayed, M. A. *J. Chem. Phys.* **1992**, *96*, 856.

(13) Freitas, J. E.; Hwang, H. J.; El-Sayed, M. A. *J. Phys. Chem.* **1994**, *98*, 3322.

(14) Dietz, T. D.; Duncan, M. A.; Liverman, M. G.; Smalley, R. E. *J. Chem. Phys.* **1980**, *73*, 4816.

(15) Pence, W. H.; Baughcum, S. L.; Leone, S. R. *J. Phys. Chem.* **1981**, *85*, 3844.

(16) O'Brien, S. C.; Kittrell, C.; Kinsey, J. L.; Johnson, B. R. *J. Chem. Phys.* **1992**, *96*, 67.

(17) Cheng, P. Y.; Zhong, D.; Zewail, A. H. *Chem. Phys. Lett.* **1995**, *237*, 399.

(18) Zhong, D.; Zewail, A. H. *J. Chem. Phys.* **1998**, *102*, 4031.

(19) Tembreull, R.; Sin, C. H.; Li, P.; Pang, H. M.; Lubman, D. M. *Anal. Chem.* **1985**, *57*, 1186.

(20) Matsumoto, J.; Lin, C.-H.; Imasaka, T. *Anal. Chem.* **1997**, *69*, 4529.

(21) Wilkerson, C. W.; Reilly, J. P. *Anal. Chem.* **1990**, *62*, **2**, 1804.

(22) Eppink, A. T. J. B.; Parker, D. H. *J. Chem. Phys.* **1998**, *109*, 4578.

(23) Sato, Y.; Matsumi, Y.; Kawasaki, M.; Tsukiyama, K.; Bersohn, R. *J. Phys. Chem.* **1995**, *99*, 16307.

(24) Baerends, E. J.; Ellis, D. E.; Ros, P. *Chem. Phys.* **1973**, *2*, 41.

(25) Ravenek, W. In *Algorithms and Applications on Vector and Parallel Computers*; Riele, H. J. J. T., Dekker, T. J., Van de Vorst, H. A., Eds.; Elsevier: Amsterdam, 1987.

(26) Boerrigter, P. M.; Velde, G. T.; Baerends, E. J. *Int. J. Quantum Chem.* **1988**, *33*, 87.

(27) Velde, G. T.; Baerends, E. J. *J. Comput. Phys.* **1992**, *99*, 84.

(28) Fan, L.; Ziegler, T. *J. Chem.* Phys. **1991**, *94*, 6057. (b) Fan, L.; Ziegler, T. *J. Chem. Phys.* **1991**, *95*, 7401. (c) Fan, L.; Versluis, L.; Ziegler, T.; Baerends, E. J.; Ravenek, W. *Int. J. Quantum Chem.* **1988**, *S22*, 173. (d) Fan, L.; Ziegler, T. *J. Chem. Phys.* **1992**, *96*, 9005. (e) Fan, L.; Ziegler, T. *J. Phys. Chem.* **1992**, *96*, 6937.

(29) Vosko, S. H.; Wilk, L.; Nusair, M. *Can. J. Phys.* **1980**, *58*, 1200.

(30) Becke, A. D. *Phys. Rev. A* **1988**, *38*, 2398.

(31) Perdew, J. P. *Phys. Rev. B* **1986**, *33*, 8822; *34*, 7046.

(32) Snijders, J. G.; Baerends, E. J.; Ros, P. *Mol. Phys.* **1978**, *36*, 1789. (b) Snijders, J. G.; Baerends, E. J.; Ros, P. *Mol. Phys.* **1979**, *36*, 1969.

(33) Schreckenbach, G.; Ziegler, T.; Li, J. *Int. J. Quantum Chem., Quantum Chem.* **1995**, *56*, 477.

(34) Snijders, J. G.; Baerends, E. J.; Vernooijs, P. *At. Nucl. Data Tables* **1982**, *26*, 483. (b) Vernooijs, P.; Snijders, G. J.; Baerends, E. J. *Slater Type Basis Functions for the whole Periodic System*; Internal Report; Free University of Amsterdam: Amsterdam, The Netherlands, 1981.

(35) Krijn, J.; Baerends, E. J. *Fit Functions in the HFS-method*; Internal Report (in Dutch); Free University of Amsterdam: Amsterdam, The Netherlands, 1984.

(36) For the hydrogen halides, the equivalent parallel transition is to the $a^3\Pi_0(e,f)$ states. The odd (f) parity state correlates adiabatically with $I(^2P_{3/2})$, whereas for even (e) parity the adiabatic product is $I(^2P_{1/2})$.

(37) Kumaran, S. S.; Su, M.-C.; Michael, J. V. *Chem. Phys. Lett.* **1997**, *269*, 99.

(38) This value is an upper bound, inasmuch as the vibrational temperature of iodobenzene in the pulsed beam is likely to be <298 K. E_{int}^p has values of 1.3, 0.8, 0.4, and 0.1 kcal/mol at 250, 200, 150, and 100 K, respectively.

(39) Trentelman, K. A.; Kable, S. H.; Moss, D. B.; Houston, P. L. *J. Chem. Phys.* **1989**, *91*, 7498.

(40) Busch, G. E.; Wilson, K. R. *J. Chem. Phys.* **1972**, *56*, 3626.

(41) Zhang, H.; Zhu, R. S.; Wang, G. J.; Sun, J. L.; Han, K.; He, G. Z.; Lou, N. Q. *Sci. China, Ser. B* **1999**, *42*, 305.

(42) The larger values of E_{avl} cited in ref 11 result from the authors' assumption of an older and smaller value for D_0^0 and a larger value for E_{int}^p.

(43) Syage, J. S. *J. Chem. Phys.* **1990**, *92*, 1804.

(44) Tanaka, Y.; Kawasaki, M.; Matsumi, Y. *Bull. Chem. Soc. Jpn.* **1998**, *71*, 2539.

(45) Chandler, D. W.; Parker, D. H. *Adv. Photochem.* **1999**, *25*, 59.

(46) Sakai, H.; Safvan, C. P.; Larsen, J. L.; Hilligsøe, K. M.; Hald, K.; Stapelfeldt, H. *J. Chem. Phys.* **1999**, *110*, 10235.

(47) Yim, Y. H.; Kim, M. S. *J. Phys. Chem.* **1993**, *97*, 12122.

(48) Samartzis, P. C.; Bakker, B. L. G.; Parker, D. H.; Kitsopoulos, T. N. *J. Phys. Chem. A* **1999**, *103*, 6106.

(49) Klots, C. E. *Z. Naturforsch.* **1971**, *27A*, 553.

(50) We thank Prof. William Hase for the use of his RRKM program.

(51) See for example: Choe, J. C.; Kim, M. S. *J. Phys. Chem.* **1991**, *95*, 50.

(52) This value is based on a C−I bond energy of 67.6 kcal/mol and an ionization potential of 200.3 kcal/mol for neutral iodobenzene.

(53) Apart from an arbitrary scale factor, the phase space calculation for photodissociation of the parent is indistinguishable from the curves shown in Figure 11.

(54) We thank Dr. Willem Siebrand for bringing this point to our attention.

(55) Henry, B. R.; Siebrand, W. *J. Chem. Phys.* **1968**, *49*, 5369.

(56) Unny, S.; Du, Y.; Zhu, L.; Truhins, K.; Gordon, R. J.; Sugita, S.; Kawasaki, M.; Matsumi, Y.; Delmdahl, R.; Parker, D. H.; Berces, A. *Phys. Rev. Lett.* (in press).

(57) Unny, S.; Zhu, L.; Truhins, K.; Gordon, R. J. Unpublished results.

(58) Kouchi, N.; Ukai, M.; Hatano, Y. *J. Phys. B: At. Mol. Opt. Phys.* **1997**, *30*, 2319.

(59) He, Z. X.; Cutler, J. N.; Southworth, S. H.; Hughey, L. R.; Samson, J. A. R. *J. Chem. Phys.* **1995**, *103*, 3912. (b) Ito, K.; Lablanquie, P.; Guyon, P.; Nenner, I. *Chem. Phys. Lett.* **1988**, *151*, 121. (c) Latimer, C. J.; Irvine, A. D.; McDonald, M. A.; Savage, O. G. *J. Phys. B: At. Mol. Opt. Phys.* **1992**, *25*, L211. (d) Latimer, C. J.; Dunn, K. F.; O'Neill, F. P.; McDonald, M. A.; Kouchi, N. *J. Chem. Phys.* **1995**, *102*, 722.

(60) Bakker, B.; Parker, D. H.; van der Zande, W. Submitted for publication.

(61) Davies, J. A.; LeClaire, J. R.; Continetti, R. E.; Hayden, C. C. *J. Chem. Phys.* **1999**, *111*, 1.

(62) Gordon, R. J.; Hall, G. E. *Adv. Chem. Phys.* **1996**, *96*, 1.